



COVID-19 pneumonia: Perfusion abnormalities shown on subtraction CT angiography in apparently well-ventilated lungs. A prospective cohort study

Mario G. Santamarina^{a,b,*}, Felipe Martinez Lomakin^{c,d}, Ignacio Beddings^e, Dominique Boisier Riscal^c, Jose Chang Villacís^f, Roberto Contreras^f, Jaime Vidal Marambio^c, Eduardo Labarca^c, Jorge Torres^a, Mariano Volpacchio^g

^a Radiology Department, Hospital Naval Almirante Nef, Viña del Mar, Chile

^b Radiology Department, Hospital Dr. Eduardo Pereira, Valparaiso, Chile

^c Intensive Care Unit, Hospital Naval Almirante Nef, Viña del Mar, Chile

^d Universidad Andrés Bello, Viña del Mar, Escuela de Medicina, Facultad de Medicina Viña del Mar, Valparaiso, Chile

^e Radiology Department, Hospital Clínico San Borja Arriaran, Santiago, Chile

^f Intensive Care Unit, Hospital San Martín de Quillota, Quillota, Chile

^g Radiology Department, Centro de Diagnóstico Dr. Enrique Rossi, Buenos Aires, Argentina

ARTICLE INFO

Keywords:

COVID-19

Computed tomography angiography

Angiotensin converting enzyme 2

Vasoconstriction

Ventilation-perfusion ratio

ABSTRACT

Purpose: To evaluate whether a subtraction CT angiography (sCTA) perfusion score may have prognostic value in patients with COVID-19 pneumonia.

Method: This prospective cohort study included adult patients with RT-PCR-confirmed SARS-CoV-2 infection admitted to the ED and a sCTA performed within 24 h of admission between June and September 2020. Perfusion abnormalities (PA) in areas of apparently spared lung parenchyma on conventional CT images were assessed with sCTA perfusion score. Airspace disease extension was assessed with CT severity scores, which were then correlated with clinical outcomes (admission to ICU, requirement of IMV, and death). Inter-rater reliability (IRR) was assessed using Cohen's Kappa. Independent predictors of adverse outcomes were evaluated by multivariable logistic regression analyses using the Hosmer and Lemeshow's test.

Results: 191 patients were included: 112 males (58%), median age of 60.8 years (SD ± 16.0). The IRR was very high (median Kappa statistic: 0.95). No association was found between perfusion CT scores and D-dimer levels (Kendall's Tau-B coefficient = 0.08, p = 0.16) or between PaO₂/FiO₂ ratios and D-dimer levels (Kendall's Tau-B coefficient = -0.10, p = 0.07). Multivariate analyses adjusting for parenchymal disease extension, vascular beaded appearance, pulmonary embolism, sex, and age showed that severe PA remained a significant predictor for ICU admission (AOR: 6.25, 95% CI 2.10–18.7, p = 0.001). The overall diagnostic capacity of this model was adequate (ROC AUC: 0.83; 95% CI 0.77–0.89).

Conclusions: The assessment of pulmonary perfusion abnormalities in areas of apparently spared lung parenchyma on conventional CT images via sCTA perfusion scoring has prognostic value in COVID-19 pneumonia.

* Corresponding author. Radiology Department, Hospital Naval Almirante Nef, Viña del Mar, Chile.

E-mail address: mgsantama@yahoo.com (M.G. Santamarina).

1. Introduction

Rapid progression to acute hypoxemic respiratory failure has been reported in up to 20% of COVID-19 pneumonia cases [1]. Severe gas exchange impairment can occur even in early stages with only minor lung airspace disease [2–4]. This may suggest that the shunt associated with the gasless lung parenchyma is not sufficient to explain hypoxemia.

Angiotensin-converting enzyme 2 (ACE2) is widely distributed in the endothelium [5]. ACE2 is an essential regulator of the renin-angiotensin system (RAS) and plays an essential role in maintaining endothelial integrity [6]. SARS-CoV-2 binds to the endothelial ACE2 receptor and produces an imbalance of RAS that is key to understanding the perfusion abnormalities (PA) that occur in COVID-19 pneumonia [7,8]. Although some authors have suggested that microthrombi can explain the perfusion deficits [9], it is likely that these microthrombi occur late in the course of the disease when the balance between thromboinflammatory responses and fibrinolytic activity is lost and a pro-coagulant state ensues [8].

In this prospective cohort, we evaluated and quantified lung PA in areas of apparently well-ventilated lung parenchyma (AWVP) in conventional chest CT images in patients with COVID-19 pneumonia via a subtraction CT angiography (sCTA) perfusion score. We also correlated PA with clinical outcomes and D-dimer levels. The aim of this study was to evaluate whether the sCTA perfusion score may have prognostic utility in patients with COVID-19 pneumonia.

2. Materials and methods

During the course of the pandemic, routine use of sCT angiography was established as standard practice in both study centers. This approach was selected in order to assess the presence of pulmonary embolism associated with COVID-19, given the thromboinflammatory nature of the disease. Images from consecutively enrolled patients were prospectively collected and archived in a database, which was made available in an anonymized form to the research team. Given the observational nature of our study, the need for informed consent was waived by the Institutional Review Board of the Hospital Naval Almirante Nef, Chile (Nr. 6025/731). We recruited adult patients (>18 years old) with SARS-CoV-2 infection confirmed by real-time reverse transcription polymerase chain reaction (RT-PCR) admitted to the emergency department and who had a chest CTA scan with post-processing iodine distribution maps performed within 24 h of admission. These subjects were consecutively enrolled at two tertiary hospitals between 1 June and 30 September 2020. A basic clinical and demographic profile was obtained in all cases.

All participants were followed-up until hospital discharge while monitoring for the development of any of the study outcomes. These outcomes included intensive-care unit (ICU) admission, initiation of invasive mechanical ventilation (IMV), and death. The decision to intubate or admit to an ICU facility was left to the attending physician's discretion.

2.1. CTA image acquisition and interpretation

Due to the prothrombotic state that has been commonly described amongst patients with SARS-CoV-2 infections, sCTA was established as a standard imaging procedure for patients that were hospitalized with COVID-19 at both study centers in order to rule out pulmonary embolism at baseline. Imaging data were acquired with multidetector-CT (Canon Aquilion Prime 80, and Canon Aquilion RXL 16, Canon Medical Systems, Japan). CTA scan protocols are in the Supplemental Material. Iodine distribution maps of the early and delayed arterial phases were obtained using SureSubtraction software (version 7.0; Canon Medical Systems, Japan).

Baseline lung CT characteristics were recorded such as the predominant imaging pattern, extension of involved lung, presence of pleural effusion, evidence of right-ventricular overload, and pulmonary embolism (PE). The areas of injured parenchyma in both lungs were assessed for a predominant pattern. These were characterized as ground glass opacities, consolidation, and mixed patterns. Airspace disease was assessed for each of the five lobes considering the extent of anatomic involvement. The resulting CT severity score was the sum of each individual lobar score (range: 0–15), and a detailed explanation of the analysis is provided in the Supplemental Material. Peripheral vascular dilatation—defined as an increased diameter of 1.5 times the accompanying bronchus or lack of tapering—and vascular beaded appearance—defined as areas of small fusiform or saccular-appearing dilatation of subsegmental pulmonary vessels—were also assessed.

Hypoperfusion in AWVP on conventional CTA images was qualitatively assessed to determine the presence and extent of hypoperfusion. Iodine distribution maps were created by subtracting the non-contrast-enhanced CT series from both the angiographic and delayed arterial contrast-enhanced CT series. This resulted in each patient having two different stacks of iodine distribution maps of their lung parenchyma. Radiologists assessed both stacks and chose the one with the least artifacts and the most uniform iodine distribution to carry out the assessment of hypoperfusion for each patient. The same stack that was selected for assessing the iodine distribution color map was later used for quantitative analysis of contrast enhancement. Hypoperfusion was considered to be present when the iodine distribution color maps are similar to the zone of the scale that contains purple-bluish hues in areas of well-aerated lung parenchyma. Well-aerated lung parenchyma that showed more adequate perfusion showed yellow or orange hues. Normally expected anteroposterior and apicobasal perfusion gradients and baseline reference perfusion patterns of patients without PA were determined using a sCTA perfusion score (Figure A1). First, both lungs were divided into five lobes (right upper lobe, middle lobe, lower right lobe, left upper lobe and left lower lobe). Then, the extension of hypoperfusion in AWVP in each lobe was categorized as “normal perfusion” (0 points), “less than 50% of the lobe affected” (1 point), and “50% of the lobe or more affected” (2 points). This resulted in an overall score that ranged from 0 to 10 points with higher scores indicating more severe hypoperfusion in areas of AWVP.

Patients were divided into three groups: Patients with three points or less were considered to have mild PA, those with 4–6 points

had moderate PA, and those with 7 or more points had severe PA.

Enhancement of the pulmonary parenchyma in AWVP also was quantified using the open-source 3D Slicer software (4.13.0-2022-03-02 r30670/09c0f73, <https://www.slicer.org>) [10]. We obtained the mean and median difference in Hounsfield Units (HU) between the non-contrast and contrast-enhanced series and then correlated it with the sCTA perfusion score. A detailed explanation of this evaluation is provided in the appendix.

Conventional CTA and sCTA features were recorded in an anonymized registry.

Inter-rater reliability was assessed using Cohen's Kappa in a subsidiary sample of 45 sCTA scans. Two radiologists, one with 7 years of experience in general and musculoskeletal radiology (IB), and another with 18 years of experience in thoracic radiology (MS), were unaware of the original radiology report and both clinical and laboratory findings. The attending physicians did not have information regarding sCTA perfusion results. However, data regarding the overall CT characteristics of the included participants was made available to clinicians in the radiology reports per current protocols at study centers.

2.2. Statistical analysis

2.2.1. Sample size

We used previous data from earlier research regarding sCTA findings amongst patients with COVID-19 [3] to estimate that 190 patients would provide the 80% statistical power. This calculation assumed a HR of 2.0 for ICU admission amongst patients with severe PA, an ICU admission rate of 15%, and a two-sided p-value of 5%. The target sample size was increased by an additional 10% to account for artifacts that might render sCTA results uninterpretable.

2.2.2. Analysis plan

Descriptive statistics including medians, means, standard deviations, interquartile ranges (IQR), and absolute and relative frequencies were used to describe participant characteristics. Bivariate comparisons between groups were performed using Fisher's exact test for categorical variables and one-way analysis of variance (ANOVA) or Kruskal-Wallis' test for continuous variables after reviewing data distribution and variances. Associations between quantitative variables were determined using Kendall's correlation coefficient.

A maximum likelihood multivariable logistic regression model was used to both quantify the association between PA and the need

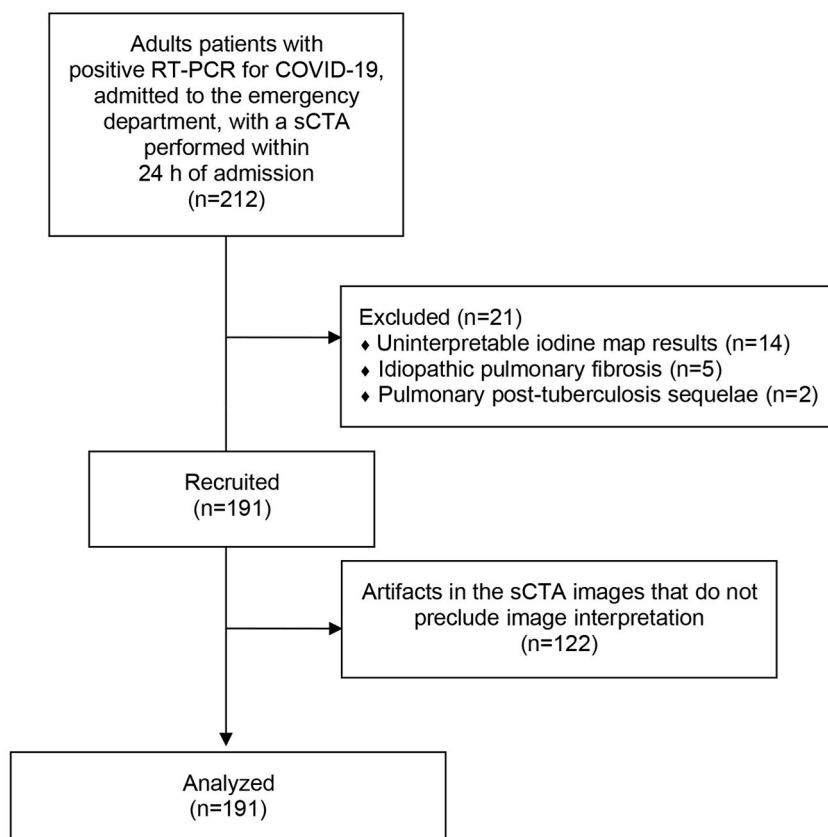


Fig. 1. Study flow chart.

for intensive care unit admission and control for relevant confounders. All candidate models were developed considering potential associations between independent variables in their development. The overall goodness of fit of the model was evaluated using Hosmer and Lemeshow's statistic, and its diagnostic accuracy was assessed using receiver operating characteristics (ROC) curves. All tests were conducted by an independent statistician who had no participation in the decision to admit or intubate any of the patients. This step used STATA 16.1 SE® (College Station, TX: StataCorp LLC). A two-sided p-value of <5% was considered to be statistically significant.

3. Results

3.1. Baseline demographic and clinical characteristics of patients

There were 212 patients in this cohort, but 21 patients were excluded: 5 due to idiopathic pulmonary fibrosis, 2 due to pulmonary post-tuberculosis sequelae and 14 (6.8% 95% CI 3.7%–11.2%) due to uninterpretable iodine map results (Figure A2) (Fig. 1). 191 patients were included: 112 males (58%), median age of 60.8 years (SD ± 16.0), and the median duration of symptoms was 8 (IQR 5–12) days (Table 1). The median Sequential Organ Failure Assessment (SOFA) score on admission was two (IQR 0–2), and the average PaO₂/FiO₂ ratio on admission was 250 ± 118. Patients with severe PA showed significantly higher SOFA scores and lower PaO₂/FiO₂ ratios than individuals with mild or moderate anomalies (Kruskall-Wallis p < 0.001 for both comparisons) (Fig. 2).

3.2. Pulmonary CT evaluation

The agreement between both radiologists was very high with a median Kappa statistic of 0.95. The domain with least consensus between observers was vascular tortuosity ($\kappa = 0.9$). Evidence of PE had the highest level of agreement ($\kappa = 1.0$).

The most common patterns seen in lung CT scans were ground-glass opacities (40.8%) followed by mixed patterns with predominant ground-glass opacities (40.8%) and mixed patterns with predominant consolidation (14.6%). A pure consolidative pattern was rare with only 3.6% of included patients showing this finding on admission. Patients with severe PA tended to show a higher frequency of consolidative patterns, but this difference was not significant (p = 0.06). The median pulmonary CT severity score was 9 (IQR 5–12) points. Table 1 shows that participants with severe PA had CT severity scores that were significantly higher than those in other groups (p < 0.001).

Signs of PE were found in 20 patients (10.5%), and all of them had an abnormal perfusion on sCTA. Most cases of PE were found amongst individuals with severe PA and localized at the segmental or subsegmental level. No association was found between perfusion CT scores and D-dimer levels (Kendall's Tau-B coefficient = 0.08, p = 0.16) or between PaO₂/FiO₂ ratios and D-dimer levels (Kendall's Tau-B coefficient = -0.10, p = 0.07). Patients with PE detected in CT had a rise of D-dimer levels 5.5-fold the normal maximum (IQR

Table 1
Baseline characteristics.

Characteristic	Mild Perfusion Anomalies (n = 16)	Moderate Perfusion Anomalies (n = 34)	Severe Perfusion Anomalies (n = 141)	Total (n = 191)	P-Value
Clinical Characteristics					
Mean Age (years) (SD)	48.5 ± 15.5	60.2 ± 18.4	62.9 ± 14.6	60.8 ± 16.0	0.002 ^a
Male sex (n, %)	9 (56.3%)	18 (52.9%)	85 (60.3%)	112 (58.0%)	0.71 ^b
Median SOFA score (IQR)	0 (0–1)	0 (0–1)	2 (2–3)	2 (0–2)	<0.001 ^a
Median duration of symptoms (IQR)	6 (4–8)	7 (4–11)	9 (5–13)	8 (5–12)	0.06 ^a
Mean PaO ₂ /FiO ₂ ratio (SD)	363 ± 41	336 ± 91	209 ± 111	250 ± 118	<0.001 ^a
Median D-dimer level (IQR; TNL)	0.7 (0.8–2.7)	0.8 (1.1–4.0)	0.9 (1.1–3.2)	0.8 (1.5–3.2)	0.16 ^c
Computed Tomography Findings					
Predominant Pattern (n, %)					
Ground-glass opacities	11 (68.7%)	18 (52.9%)	49 (35.0%)	78 (40.8%)	
Mixed Pattern with predominant ground-glass opacities	2 (12.5%)	12 (35.3%)	64 (45.5%)	78 (40.8%)	
Mixed pattern with predominant consolidation	3 (18.8%)	3 (8.8%)	22 (15.6%)	28 (14.6%)	
Consolidation	0 (0%)	1 (2.9%)	6 (4.3%)	7 (3.6%)	
Pleural effusion (n, %)	0 (0%)	2 (5.9%)	14 (13.9%)	16 (8.3%)	0.55 ^b
Pulmonary embolism (n, %)	0 (0%)	2 (5.9%)	18 (12.8%)	20 (10.5%)	0.26 ^b
Right ventricular overload (n, %)	0 (0%)	0 (0%)	2 (1.4%)	2 (1.1%)	>0.99 ^b
Vascular dilatation (n, %)	7 (43.8%)	23 (67.7%)	138 (97.8%)	168 (88.0%)	<0.001 ^b
Vascular beading appearance (n, %)	3 (18.8%)	8 (23.5%)	94 (66.7%)	105 (55.0%)	<0.001 ^b
Median CT Severity Score (IQR)	5 (3–5)	5 (4–6)	10 (8–12)	9 (5–12)	<0.001 ^a

SD: Standard Deviation.

IQR: Interquartile range.

SOFA: Sequential Organ Failure Assessment.

TNL: Times over upper normal limit.

^a One-way Analysis of Variance (ANOVA).

^b Fisher's Exact Test.

^c Kruskal-Wallis rank sum test.

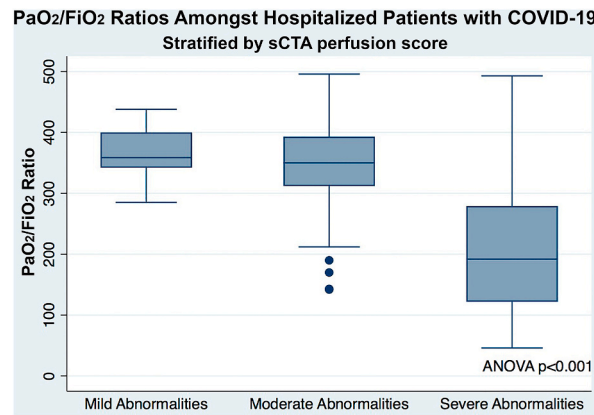


Fig. 2. PaO₂/FiO₂ ratios amongst hospitalized patients with COVID-19. Stratified by sCTA Perfusion Score.

2.8–17.5); those who did not have PE had a mean of 1.4-fold in D-dimer (IQR 0.76–3.0 times; $p < 0.001$). Pleural effusion was rare in the participants (16 patients, 8.3%); only two patients (1.1%) showed signs of right ventricular overload. Both were in the severe PA group.

Vascular dilatation and vascular beaded appearance were observed in 168 (88%) and in 105 patients (55%) respectively, in areas of airspace disease. Most cases were found in the severe PA group (94 patients, 66.7%) (Fig. 3). The presence of vascular beaded appearance was significantly associated with admission to an ICU (OR: 4.6, 95% CI 2.40–8.70, $p < 0.001$), requirement of IMV (OR 5.3, 95% CI 2.4–12.0, $p < 0.001$), and in-hospital mortality (OR 2.4, 95% CI 1.02–5.4, $p = 0.04$).

3.3. Perfusion findings and study outcomes

PA was common amongst included participants with 189 (98.9%) patients having abnormal results. The morphology of PA was predominantly regional and non-lobular. We found artifacts in 63.8% (122/191) of the iodine map images, but these artifacts were not severe enough to preclude image interpretation (Fig. 4).

In AWVP, the median sCTA perfusion score was 9 points (IQR 6–10). Patients were then categorized in three groups using the aforementioned scoring system. Sixteen patients (8.4%) were identified as having mild PA, 34 patients (17.8%) had moderate PA, and 141 (73.8%) had severe PA (Fig. 5). In the quantitative analysis, the mean and median attenuation values of iodine enhancement in AWVP (lung perfusion blood volume) in patients having mild PA were 29.8 HU (SD 14.7) and 35.9 HU (SD 17.1); moderate PA were 22.6 HU (SD 9.9) and 27.5 HU (SD 11.6); and severe PA were 10.0 HU (SD 7.5) and 12.7 HU (SD 9.0), respectively ($p < 0.001$). The mean percentage of emphysema was $0.38 \pm 0.57\%$ without any differences between perfusion groups (ANOVA $p = 0.0025$). A significant correlation was found between the extent of lung parenchymal disease and PA (Kendall Tau B = 0.50, $p < 0.001$).

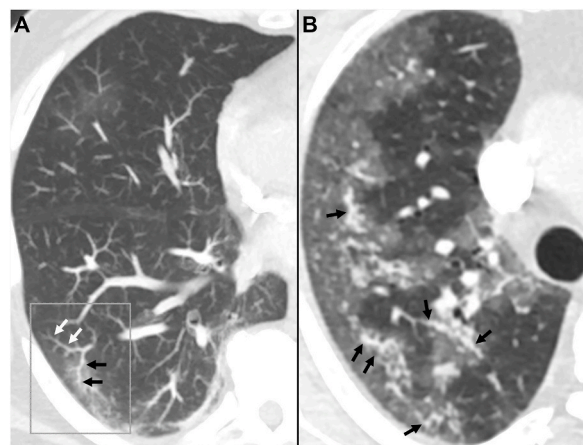


Fig. 3. Pulmonary vascular abnormalities. A. Vascular dilatation. MIP CTA axial image shows lack of tapering of subsegmental pulmonary vessels (black arrows) running through an area of ground-glass opacity. Another contiguous vascular branch is evidenced with the expected normal tapering (white arrows). B. Vascular beading appearance. Axial CTA image shows significant and extensive fusiform or saccular-appearing dilatation of subsegmental pulmonary vessels (black arrows). This 62-year-old man had 5 days since symptom onset, was initially admitted to the ICU, managed with IMV and died 3 weeks after admission.

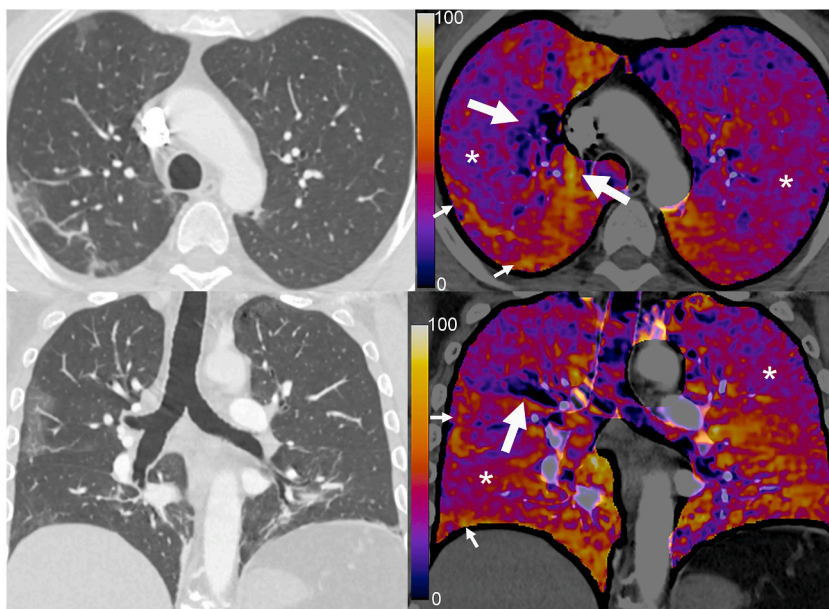


Fig. 4. Hard beam artifacts. Conventional and color map sCTA axial and coronal images. 62-year-old male patient. 6 days since symptom onset. PaO₂/FiO₂ ratio was 298. Moderate hypoperfusion area in apparently normal lung parenchyma (*). Right lung subpleural ground-glass opacities show increased perfusion within the opacities (small arrows). Streak artifacts due to beam hardening by highly concentrated contrast in the superior vena cava (large arrows). (For interpretation of the references to color in this figure legend, the reader is referred to the Web version of this article.)

Seventy-seven patients (40.3%, 95% CI 33.3%–47.6%) were admitted to the ICU during follow up, and 44 (24.8%, 95% CI 18.7%–31.3%) required IMV. Thirty patients (14.6%, 95% CI 10.0%–20.5%) died during hospitalization. None of the patients with normal perfusion CT scans required admission to the ICU or IMV, and both survived their hospitalization. In addition, none of the patients with mild PA required IMV.

Patients with severe PA were more likely to be admitted to an intensive care facility, require mechanical ventilation, or showed decreased in-hospital survival. When contrasted to patients with mild disease, the unadjusted odds ratio for ICU admission in patients with severe PA was 11.6 (95% CI 4.3–31.4, $p < 0.001$) and 23.2 (95% CI 3.1–174.4, $p = 0.0062$) for IMV requirements. Twenty-five patients in the severe PA group (17.7%) died during the hospitalization, which translated in an OR of 5.23 (95% CI 1.2–23.0, $p = 0.04$) for mortality. A summary of study outcomes is shown in [Table 2](#).

A multivariable logistic regression model was constructed using ICU admission as the outcome variable: Lung PA scoring 7 or more points remained a significant predictor of ICU admission after adjustments for parenchymal disease extension, vascular beaded appearance, PE, sex, and age. The adjusted odds ratio was 6.25 (95% CI 2.10–18.7, $p = 0.001$). The overall diagnostic capacity of this model was good with a ROC AUC of 0.83 (95% CI 0.77–0.89) ([Fig. 6](#)); this is shown in [Table 3](#).

4. Discussion

In this prospective cohort study, we assessed perfusion alterations in AWVP on conventional CTA images in patients with COVID-19 pneumonia with the sCTA perfusion score. A preliminary cohort study was hampered due to its inability to control for relevant clinical confounders due to its limited sample size and lack of inter-observer variability assessment [3]. In this larger study, we confirmed that there is a strong correlation between increasing severity of PA and clinical outcomes. Severe PA remained a significant predictor of ICU admission after adjustments for parenchymal disease extension, vascular beaded appearance, PE, sex, and age (AOR: 6.25, 95% CI 2.10–18.7, $p = 0.001$; ROC AUC of 0.83, 95% CI 0.77–0.89). The observed agreement between two radiologists was very high with a median Kappa statistic of 0.95.

We found a strong association between the sCTA perfusion score and the quantification of iodine enhancement level (corresponding to lung perfusion blood volume) in areas of well-ventilated parenchyma. The difference in HU between the unenhanced and the contrast-enhanced series was larger in patients with mild PA than in those with severe PA ($p < 0.001$). This translates into significantly less contrast enhancement in AWVP in patients with qualitatively severe perfusion abnormalities. There was good correlation between qualitative CT perfusion scores and quantitative perfusion assessment.

SARS-COV-2 binds to ACE2 when the virus spreads to the pulmonary blood circulation. Both angiotensin I (Ang I) and angiotensin II (Ang II) accumulate due to viral blockade and down-regulation [5]. Angiotensin-converting enzyme (ACE) is not engaged by the virus, and the conversion of Ang I to Ang II continues unabated eventually leading to unopposed accumulation of Ang II [5,6]. Ang II produces vasoconstriction and endothelial dysfunction with less production of nitric oxide in early phases of disease, leading to a progressive V/Q mismatch with extensive areas of apparently healthy but hypoperfused lung that function as alveolar dead space [6,8,

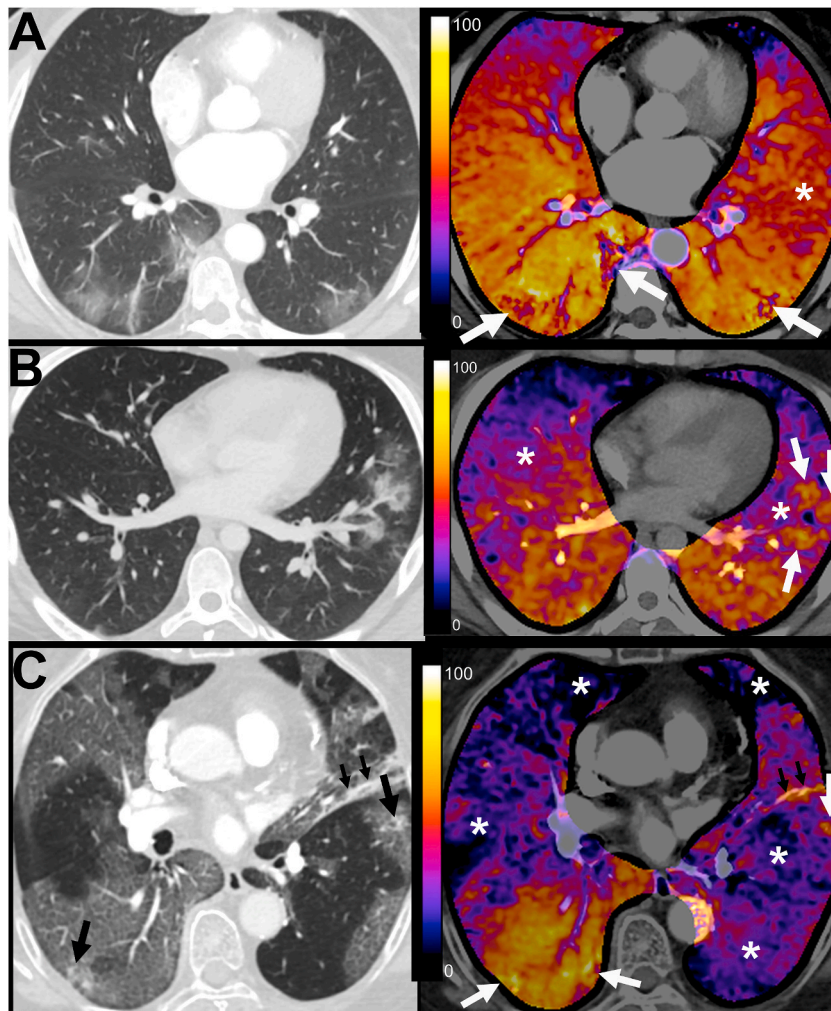


Fig. 5. Perfusion abnormalities. A. Mild perfusion abnormalities. 65-year-old female patient, 10 days since symptom onset. PaO₂/FiO₂ ratio was 390. Slight increase in D-dimer (rise of 1.36-fold the normal maximum). Outpatient management and no requirement of supplemental oxygen support. Mild hypoperfusion area in apparently normal lung parenchyma (*). Ground-glass opacities in both inferior lobes show decreased perfusion within the opacity, with a peripheral halo of increased perfusion (white arrows). These findings could be explained by physiological hypoxic vasoconstriction. B. Moderate perfusion abnormalities. 21-year-old male patient, 4 days since symptom onset. PaO₂/FiO₂ ratio was 400. Moderate increase in D-dimer (rise of 1.91-fold the normal maximum). Outpatient management and admission to the hospital 2 days later with PaO₂/FiO₂ ratio 190. Admitted to the ICU, managed with IMV. Initially, the patient presented mild involvement of the pulmonary parenchyma, moderate perfusion abnormalities in apparently normal lung parenchyma (*) and prominent areas of increased perfusion in relation to the zones of ground-glass opacities (white arrows). C. Severe perfusion abnormalities. 76-year-old female patient, 7 days since symptom onset. PaO₂/FiO₂ ratio was 117. Moderate increase in D-dimer (rise of 1.96-fold the normal maximum). Admitted to the ICU, managed with IMV. She died 3 weeks after admission. Extensive lung involvement with patchy ground-glass opacities in both lungs with right predominance, with vascular dilatation in small peripheral subsegmental pulmonary arterial branches, some of them with a varicose appearance (black arrows). Severe perfusion abnormalities in apparently normal lung parenchyma (*) and in some areas with ground glass opacities. Some areas of ground-glass opacities show marked hyperperfusion, most probably due to vasoplegia (white arrows). Note that in some ground glass opacities there are hypoperfusion areas that could be explained by microthrombosis or more likely by endothelial dysfunction. Linear atelectasis with increased perfusion in lingular segment (small black arrows).

Table 2
Study outcomes.

Outcome	Mild Anomalies (n = 16)	Moderate Anomalies (n = 34)	Severe Anomalies (n = 141)	p-value ^a
Admission to intensive care unit (n, %)	2 (12.5%)	3 (8.8%)	68 (48.2%)	<0.001
Initiation of mechanical ventilation (n, %)	0 (0%)	1 (2.9%)	40 (28.3%)	<0.001
Death (n, %)	1 (6.25%)	1 (2.9%)	25 (17.7%)	0.04

^a Simple logistic regression.

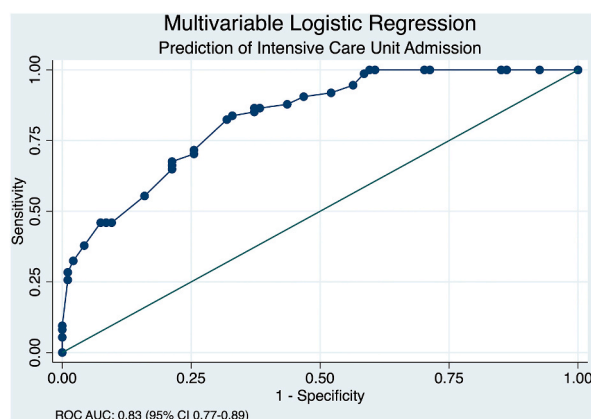


Fig. 6. Multivariable logistic regression. Prediction of Intensive Care Unit Admission.

Table 3

Multivariable logistic regression.

Variable	Adjusted Odds Ratio	95% Confidence Interval	p-value
Perfusion Score ≥ 7 points	6.25	2.1–18.7	0.001
Extension Score ≥ 11 points	4.40	1.84–10.3	0.001
Male Gender	0.58	0.26–1.30	0.19
Age ≥ 65 years	0.36	0.15–0.85	0.02
Vascular Tortuosity	2.07	0.92–4.65	0.08
Pulmonary Embolism	2.91	0.68–12.5	0.08
Constant (a)	0.22	0.05–0.92	0.04

11].

We found that patients with severe PA showed significantly higher SOFA scores and lower PaO₂/FiO₂ ratios than people with mild or moderate anomalies (ANOVA $p < 0.001$ for both comparisons). We found severe hypoxemia in several patients without significant airspace compromise, a finding that has also been mentioned in other reports [4,12,13].

We found no association between sCTA perfusion score and D-dimer levels (Kendall's Tau-B coefficient = 0.08, $p = 0.16$) or between PaO₂/FiO₂ ratios and D-dimer levels (Kendall's Tau-B coefficient = -0.10 , $p = 0.07$). Patients with PE detected in CT had a rise of D-dimer levels 5.5-fold the normal maximum (IQR 2.8–17.5); those who did not have it had a mean D-dimer level 1.4 times the normal maximum (IQR 0.76–3.0 times); this difference is highly significant ($p < 0.001$). It is likely that in non-severe and initial disease, hypoperfusion in well-ventilated lung parenchyma could be due to a dysregulation of perfusion rather than the presence of microthrombi [13]. As the infection spreads, SARS-CoV-2 develops a thromboinflammatory response with formation of thrombi and microthrombi that are initially broken down by the highly active fibrinolytic function. In severely ill patients, however, the pulmonary coagulation system becomes markedly activated above the capacity of the fibrinolytic system, which can manifest with the visualization of thrombi. This leads to increased oxygen requirements and elevated D-dimer levels [8,14,15]. These findings are consistent with some studies showing that the risk of thrombotic complications increases with COVID-19 severity [16,17]. Pulmonary embolism is a phenomenon that might affect the interpretation of perfusion CT scans. We chose to include this variable in our logistic model in order to account for it as a potential source of bias, even though no evidence of a statistically significant association was found in the final model (aOR 2.5, 95% CI 0.68–12.5, $p = 0.08$). Patients with small airway disease can also develop a V/Q mismatch with initial hypoventilation and secondary vasoconstriction [18]. The predominantly regional and non-lobular morphology of the areas of hypoperfusion, the practical absence of pulmonary emphysematous destruction observed in the quantitative analysis [19], and the lack of pathological findings of small airway disease in the early stages of infection [20] suggests that dysregulation of lung perfusion in AWVP could be the main cause of hypoperfusion, playing a key role in the development of oxygenation impairment, and should be considered in the potential therapeutic management of COVID-19 pneumonia [21].

A vascular beaded appearance [22] was significantly associated with ICU admission (OR: 4.6, 95% CI 2.40–8.70, $p < 0.001$), requirement of IMV (OR 5.3, 95% CI 2.4–12.0, $p < 0.001$) and in-hospital mortality (OR 2.4, 95% CI 1.02–5.4, $p = 0.04$). This vascular injury could be explained by local pulmonary endothelitis that occurs in areas where there is airspace disease, finally producing vasodilation that results in high perfusion to areas of hypoventilated lung developing an abnormally low V/Q ratio that can promote hypoxemia [23–25].

These findings should eventually lead additional studies to investigate the prevalence of respiratory symptoms that a high number of long-COVID patients experienced despite the dramatic improvement of lung abnormalities usually observed on CT examinations [26]. There is some evidence that in large groups of these patients, there persists perfusion abnormalities in the absence of morphological abnormalities using dual-energy computed tomography (DECT) [27]. Also, had been detected in plasma samples,

microclots containing molecules involved in blood coagulation and fibrinolysis [28], and increased levels of inflammatory molecules [29]. These findings could be reflecting an unresolved endothelial dysfunction holding a persistent hypercoagulability.

This study does have some limitations. First, sCTA is a new postprocessing technique and thus, has not been as extensively validated as DECT [9,30–36]. The image data were generated by a single-energy CT and could not be correlated with a DECT. There are also concerns regarding potential bias and lack of quantitation resulting from subtraction of non-contrast images from contrast-enhanced images that need to be addressed. Second, sCTA imaging involves more radiation than conventional CT techniques. Third, some iodine maps were uninterpretable; 63.8% had artifacts that did not preclude their interpretation. Fourth, this dataset was obtained when there were no vaccines and the delta strain had not yet appeared. It is unclear if vaccinated patients or those with new strains will have altered perfusion in a similar way. Finally, it is unclear whether these PA are unique to COVID-19 or if they can also be found in other multifocal pneumonias and other causes of ARDS.

5. Conclusions

In conclusion, sCTA is software-based and significantly less expensive and potentially more available than costly DECT equipment. The perfusion score allowed us to correlate perfusion alterations in AWVP on conventional chest CTA images in patients with COVID-19 pneumonia at admission with clinical outcomes. Severe PA remained an independent prognostic predictor of ICU admission.

Author contribution statement

Mario G. Santamarina; Ignacio Beddings: Conceived and designed the experiments; Performed the experiments; Contributed reagents, materials, analysis tools or data; Wrote the paper.

Felipe Martinez Lomakin: Conceived and designed the experiments; Analyzed and interpreted the data; Wrote the paper.

Dominique Boiser Riscal: Conceived and designed the experiments; Contributed reagents, materials, analysis tools or data; Wrote the paper.

Jose Chang Villacís; Jorge Torres: Contributed reagents, materials, analysis tools or data.

Roberto Contreras; Jaime Vidal Marambio; Eduardo Labarca: Conceived and designed the experiments; Contributed reagents, materials, analysis tools or data.

Mariano Volpacchio: Conceived and designed the experiments; Wrote the paper.

Data availability statement

Data will be made available on request.

Declaration of competing interest

The authors declare that they have no known competing financial interests or personal relationships that could have appeared to influence the work reported in this paper.

Abbreviations

ACE2	Angiotensin-converting enzyme 2
Ang I	Angiotensin I
Ang II	Angiotensin II
AWVP	areas of apparently well-ventilated lung parenchyma
DECT	Dual-Energy Computed Tomography
HU	Hounsfield Units
ICU	intensive care unit
IMV	invasive mechanical ventilation
RAS	renin-angiotensin system
SOFA	Sequential Organ Failure Assessment
PA	Perfusion abnormalities
sCTA	subtraction CT angiography

Appendix A. Supplementary data

Supplementary data to this article can be found online at <https://doi.org/10.1016/j.heliyon.2023.e18085>.

References

- [1] Z. Wu, J.M. McGoogan, Characteristics of and important lessons from the coronavirus disease 2019 (COVID-19) outbreak in China: summary of a report of 72 314 cases from the Chinese center for disease control and prevention, *JAMA* 323 (13) (2020) 1239–1242, <https://doi.org/10.1001/jama.2020.2648>.
- [2] W.J. Guan, Z.Y. Ni, Y. Hu, W.H. Liang, et al., Clinical characteristics of coronavirus disease 2019 in China, *N. Engl. J. Med.* 382 (18) (2020) 1708–1720, <https://doi.org/10.1056/NEJMoa2002032>. Epub 2020 Feb 28.
- [3] M.G. Santamarina, D. Boisier Riscal, I. Beddings, et al., COVID-19: what iodine maps from perfusion CT can reveal-A prospective cohort study, *Crit. Care* 24 (1) (2020) 619, <https://doi.org/10.1186/s13054-020-03333-3>.
- [4] L. Gattinoni, D. Chiumello, P. Caironi, et al., COVID-19 pneumonia: different respiratory treatments for different phenotypes? *Intensive Care Med.* 46 (6) (2020) 1099–1102, <https://doi.org/10.1007/s00134-020-06033-2>. Epub 2020 Apr 14.
- [5] S.G. Ramos, B. Amanda da Cruz Rattis, G. Ottaviani, M.R. Nunes Celes, E.P. Dias, ACE2 down-regulation may act as a transient molecular disease causing RAAS dysregulation and tissue damage in the microcirculatory environment among COVID-19 patients, *Am. J. Pathol.* 191 (7) (2021) 1154–1164, <https://doi.org/10.1016/j.ajpath.2021.04.010>. Epub 2021 May 6.
- [6] F. Lovren, Y. Pan, A. Quan, et al., Angiotensin converting enzyme-2 confers endothelial protection and attenuates atherosclerosis, *Am. J. Physiol. Heart Circ. Physiol.* 295 (4) (2008) H1377–H1384, <https://doi.org/10.1152/ajpheart.00331.2008>. Epub 2008 Jul 25.
- [7] M. Hoffmann, H. Kleine-Weber, S. Schroeder, et al., SARS-CoV-2 cell entry depends on ACE2 and TMPRSS2 and is blocked by a clinically proven protease inhibitor, *Cell* 181 (2) (2020) 271–280, <https://doi.org/10.1016/j.cell.2020.02.052>. Epub 2020 Mar 5.
- [8] M.G. Santamarina, D. Boisier, R. Contreras, M. Baque, M. Volpacchio, I. Beddings, COVID-19: a hypothesis regarding the ventilation-perfusion mismatch, *Crit. Care* 24 (1) (2020) 395, <https://doi.org/10.1186/s13054-020-03125-9>.
- [9] S. Aydin, M. Kantarci, E. Karavas, E. Unver, S. Yalcin, F. Aydin, Lung perfusion changes in COVID-19 pneumonia: a dual energy computerized tomography study, *Br. J. Radiol.* 94 (1125) (2021 Sep 1), 20201380, <https://doi.org/10.1259/bjr.20201380>.
- [10] A. Fedorov, R. Beichel, J. Kalpathy-Cramer, et al., 3D slicer as an image computing platform for the quantitative imaging network, *Magn. Reson. Imaging* 30 (9) (2012 Nov) 1323–1341, <https://doi.org/10.1016/j.mri.2012.05.001>. Epub 2012 Jul 6.
- [11] Y. Jin, W. Ji, H. Yang, S. Chen, W. Zhang, G. Duan, Endothelial activation and dysfunction in COVID-19: from basic mechanisms to potential therapeutic approaches, *Signal Transduct. Targeted Ther.* 5 (1) (2020) 293, <https://doi.org/10.1038/s41392-020-00454-7>.
- [12] L. Gattinoni, S. Coppola, M. Cressoni, M. Busana, S. Rossi, D. Chiumello, COVID-19 does not lead to a "typical" acute respiratory distress syndrome, *Am. J. Respir. Crit. Care Med.* 201 (10) (2020) 1299–1300, <https://doi.org/10.1164/rccm.202003-0817LE>.
- [13] M. Busana, L. Giosa, M. Cressoni, et al., The impact of ventilation-perfusion inequality in COVID-19: a computational model, *J. Appl. Physiol.* 130 (3) (2021) 865–876, <https://doi.org/10.1152/japplphysiol.00871.2020>. Epub 2021 Jan 13.
- [14] M. Oudkerk, H.R. Büller, D. Kuijpers, et al., Diagnosis, prevention, and treatment of thromboembolic complications in COVID-19: report of the national institute for public health of The Netherlands, *Radiology* 297 (1) (2020) E216–E222, <https://doi.org/10.1148/radiol.2020201629>. Epub 2020 Apr 23.
- [15] J. Thachil, S. Agarwal, Understanding the COVID-19 coagulopathy spectrum, *Anaesthesia* 75 (11) (2020) 1432–1436, <https://doi.org/10.1111/anae.15141>. Epub 2020 Jun 15.
- [16] W.J. Jenner, R. Kanji, S. Mirsadraee, Y.X. Gue, S. Price, S. Prasad, D.A. Gorog, Thrombotic complications in 2928 patients with COVID-19 treated in intensive care: a systematic review, *J. Thromb. Thrombolysis* 51 (3) (2021) 595–607, <https://doi.org/10.1007/s11239-021-02394-7>. Epub 2021 Feb 14.
- [17] A. Di Minno, P. Ambrosino, I. Calcaterra, M.N.D. Di Minno, COVID-19 and venous thromboembolism: a meta-analysis of literature studies, *Semin. Thromb. Hemost.* 46 (7) (2020) 763–771, <https://doi.org/10.1055/s-0040-1715456>. Epub 2020 Sep 3.
- [18] R. Rodríguez-Roisin, M. Drakulovic, D.A. Rodríguez, J. Roca, J.A. Barberà, P.D. Wagner, Ventilation-perfusion imbalance and chronic obstructive pulmonary disease staging severity, *J. Appl. Physiol.* 106 (6) (2009) 1902–1908, <https://doi.org/10.1152/japplphysiol.00085.2009>. Epub 2009 Apr 16.
- [19] J.D. Schroeder, A.S. McKenzie, J.A. Zach, C.G. Wilson, D. Curran-Everett, D.S. Stinson, J.D. Newell Jr., D.A. Lynch, Relationships between airflow obstruction and quantitative CT measurements of emphysema, air trapping, and airways in subjects with and without chronic obstructive pulmonary disease, *AJR Am. J. Roentgenol.* 201 (3) (2013) W460–W470, <https://doi.org/10.2214/AJR.12.10102>.
- [20] H. Bösmüller, M. Matter, F. Fend, A. Tzankov, The pulmonary pathology of COVID-19, *Virchows Arch.* 478 (1) (2021) 137–150, <https://doi.org/10.1007/s00428-021-03053-1>. Epub 2021 Feb 19.
- [21] M.G. Santamarina, I. Beddings, F.M. Lomakin, et al., Sildenafil for treating patients with COVID-19 and perfusion mismatch: a pilot randomized trial, *Crit. Care* 26 (2022) 1, <https://doi.org/10.1186/s13054-021-03885-y>.
- [22] B.V. Patel, D.J. Arachchilage, C.A. Ridge, et al., Pulmonary angiopathy in severe COVID-19: physiologic, imaging, and hematologic observations, *Am. J. Respir. Crit. Care Med.* 202 (5) (2020) 690–699, <https://doi.org/10.1164/rccm.202004-1412OC>.
- [23] M.Z. Tay, C.M. Poh, L. Rénia, P.A. MacAry, L.F.P. Ng, The trinity of COVID-19: immunity, inflammation and intervention, *Nat. Rev. Immunol.* 20 (6) (2020) 363–374, <https://doi.org/10.1038/s41577-020-03111-8>.
- [24] M. Ackermann, S.E. Verleden, M. Kuehnel, et al., Pulmonary vascular endothelialitis, thrombosis, and angiogenesis in Covid-19, *N. Engl. J. Med.* 383 (2) (2020) 120–128, <https://doi.org/10.1056/NEJMoa2015432>. Epub 2020 May 21.
- [25] M. Lang, A. Som, D. Carey, et al., Pulmonary vascular manifestations of COVID-19 pneumonia, *Radiol. Cardiothorac. Imaging* 2 (3) (2020), e200277, <https://doi.org/10.1148/ryct.2020200277>.
- [26] G. Darcis, A. Bouquegneau, N. Maes, et al., Long-term clinical follow-up of patients suffering from moderate-to-severe COVID-19 infection: a monocentric prospective observational cohort study, *Int. J. Infect. Dis.* 109 (2021) 209–216, <https://doi.org/10.1016/j.ijid.2021.07.016>.
- [27] I. Mohamed, V. de Broucker, A. Duhamel, et al., Pulmonary circulation abnormalities in post-acute COVID-19 syndrome: dual-energy CT angiographic findings in 79 patients, *Eur. Radiol.* (2023) 1–13, <https://doi.org/10.1007/s00330-023-09618-9>.
- [28] E. Pretorius, M. Vlok, et al., Persistent clotting protein pathology in Long COVID/Post-Acute Sequelae of COVID-19 (PASC) is accompanied by increased levels of antiplasmin, *Cardiovasc. Diabetol.* 20 (1) (2021) 172, <https://doi.org/10.1186/s12933-021-01359-7>.
- [29] E. Espín, C. Yang, C.P. Shannon, et al., Cellular and molecular biomarkers of long COVID: a scoping review, *EBioMedicine* 91 (2023), 104552, <https://doi.org/10.1016/j.ebiom.2023.104552>.
- [30] M.J. Kang, C.M. Park, C.H. Lee, J.M. Goo, H.J. Lee, Dual-energy CT: clinical applications in various pulmonary diseases, *Radiographics* 30 (3) (2010) 685–698, <https://doi.org/10.1148/rg.303095101>.
- [31] I.S. Idilman, G. Telli Dizman, S. Ardali Duzgun, et al., Lung and kidney perfusion deficits diagnosed by dual-energy computed tomography in patients with COVID-19-related systemic microangiopathy, *Eur. Radiol.* 31 (2) (2021) 1090–1099, <https://doi.org/10.1007/s00330-020-07155-3>. Epub 2020 Aug 29.
- [32] M. Tamura, Y. Yamada, T. Kawakami, et al., Diagnostic accuracy of lung subtraction iodine mapping CT for the evaluation of pulmonary perfusion in patients with chronic thromboembolic pulmonary hypertension: correlation with perfusion SPECT/CT, *Int. J. Cardiol.* 243 (2017) 538–543, <https://doi.org/10.1016/j.ijcard.2017.05.006>. Epub 2017 May 4.
- [33] A. Otrakji, S.R. Digumarthy, R. Lo Gullo, E.J. Flores, J.A. Shepard, M.K. Kalra, Dual-energy CT: spectrum of thoracic abnormalities, *Radiographics* 36 (1) (2016) 38–52, <https://doi.org/10.1148/rg.2016150081>.
- [34] M. Remy-Jardin, L. Duthoit, T. Perez, et al., Assessment of pulmonary arterial circulation 3 months after hospitalization for SARS-CoV-2 pneumonia: dual-energy CT (DECT) angiographic study in 55 patients, *EClinicalMedicine* 34 (2021), 100778, <https://doi.org/10.1016/j.eclinm.2021.100778>. Epub 2021 Mar 30.
- [35] D. Grob, L.J. Oostveen, C. Jacobs, et al., Iodine maps from subtraction CT or dual-energy CT to detect pulmonary emboli with CT angiography: a multiple-observer study, *Radiology* 292 (1) (2019) 197–205, <https://doi.org/10.1148/radiol.2019182666>.
- [36] B. Dissaux, P.Y. Le Floch, P. Robin, et al., Pulmonary perfusion by iodine subtraction maps CT angiography in acute pulmonary embolism: comparison with pulmonary perfusion SPECT (PASEP trial), *Eur. Radiol.* 30 (9) (2020) 4857–4864, <https://doi.org/10.1007/s00330-020-06836-3>. Epub 2020 Apr 11.